Development of an Integrated Haptic Sensor System for Multimodal Human–Computer Interaction Using Ultrasonic Array and Cable Robot

Liqiang Fan, Aiguo Song, *Senior Member, IEEE*, and Haochen Zhang

***Abstract*—This paper presents the design and development of a novel haptic sensor system. It integrates cable-driven force and ultrasonic tactile feedback, which can produce multimodal haptic stimuli. The sensing element includes a Leapmotion, an ultrasonic transducer array, tension sensors, and rotary encoders, which are used to capture hand posture, project tactile points, measure cable force and length, respectively. Firstly, a 6-DOF cable-driven force feedback apparatus based on parallel mechanism is designed and ultrasonic phased array is combined to form a multimodal haptic feedback system. Secondly, a multimodal haptic fusion method for cable-driven force and ultrasonic tactile is firstly proposed to invoke realistic compound haptic sensations. To enhance the rendering effects of each subsystem, admittance control is developed for a cable robot, and a new perceived magnitude model is established for ultrasound tactile rendering. A psychophysical experiment is conducted to study the perceived characteristics of multimodal haptic stimuli. To verify the proposed system, a series of experiments were carried out, whose results indicated that the system performs well at multi-property haptic rendering and confirm the accuracy and sensitive advantage of our system in virtual reality applications. The results of our study indicate that this device has great application potential in human-computer interaction.**

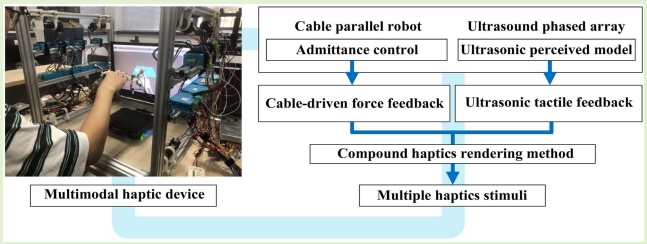

***Index Terms*—Multimodal haptic interface, cable-driven parallel force, ultrasonic tactile, haptic feedback.**

I. Introduction

THE human haptic perception system is complex, and is influenced by a variety of factors: sensory information derived from mechanoreceptors; thermoreceptors embedded in the skin (cutaneous inputs); and mechanoreceptors embedded in muscles, tendons, and joints (kinesthetic inputs). Cutaneous and kinesthetic inputs are combined and weighted in different ways to support various haptic functions [1]. Multimodal haptic systems have emerged to display more realistic haptic feedback for operators in virtual environments [2].

Based on structure characteristics, multimodal haptic devices can be classified as handheld, wearable, and desktop devices. Handheld devices have a large workspace to enable large-scale body movement [3], but the simulated gestures are relatively simple. Finger-mounted wearable devices can support diverse hand postures [4]. However, the complex structure can affect dexterity and the perceived effect when integrating different actuator elements. Desktop haptic devices have the widest range of applications, and can integrate multiple haptic elements in one compact structure [5]. High-fidelity multimodal haptic devices will become increasingly important in minimally invasive surgery [6], industrial applications [7], and human-computer interaction [8].

Ultrasound tactile technology is emerging for haptic rendering with its large workspace, high degree of freedom, and absence of direct physical contact. Ultrasound haptic stimulation has been successfully applied in biological studies since the 1980s [9]. Airborne ultrasound haptic studies conducted by the University of Tokyo have shown that ultrasonic phased arrays can project reliable tactile points for human

Manuscript received November 29, 2021; revised January 13, 2022; accepted January 17, 2022. Date of publication January 19, 2022; date of current version February 28, 2022. This work was supported in part by the National Natural Science Foundation of China under Grant U1713210. The associate editor coordinating the review of this article and approving it for publication was Prof. Kazuaki Sawada. *(Corresponding author: Aiguo Song.)*

Liqiang Fan and Aiguo Song are with the State Key Laboratory of Bioelectronics and the Jiangsu Key Laboratory of Remote Measurement and Control, School of Instrument Science & Engineering, Southeast University, Nanjing, Jiangsu 210096, China (e-mail: a.g.song@seu.edu.cn).

Haochen Zhang is with the State Key Laboratory of Bioelectronics and the Jiangsu Key Laboratory of Remote Measurement and Control, School of Instrument Science & Engineering, Southeast University, Nanjing, Jiangsu 210096, China, and also with the College of Electrical and Information Engineering, Lanzhou University of Technology, Lanzhou 730050, China.

Digital Object Identifier 10.1109/JSEN.2022.3144888

interaction [10]. Carter *et al.* developed an ultrahaptics prototype that could generate multi-points and render 3D shapes in midair [11], [12], and has been used in commercial products [13], [14]. Some researchers are committed to introducing ultrasonic array to provide multi-resolution haptic images and obtain a more natural haptic feedback effect [15], [16].

Cable-driven parallel robots were developed in the United States for industrial applications like painting, welding, and manipulation [17], as well as teleoperation systems [18] and rehabilitation [19]. The SPIDAR series has broad application prospects, with excellent force feedback accuracy, low inertia, and lightness [20]. Human-robot cooperation has become increasingly important, and is the subject of much research. Cable-driven force feedback systems were developed for haptic interaction [21], [22].

Due to technical limitations, the output pressure of the ultrasound array is relatively weak and lacks high accuracy. Weight and delicate textures are unsuitable for ultrasound tactile rendering. We hope to enhance the output pressure of focus and improve the rendering effect of ultrasonic tactile by modulating the waveform (such as using square wave). The working characteristics of ultrasound tactile determined it is easy to integrate with other haptic devices. As a force feedback device, the cable robot has a huge workspace and low inertia, which is suitable for combining with ultrasound arrays. We expect that this combination can provide benefits such as multi-resolution haptic images and a synergistic effect on haptic perception. A multimodal haptic device is developed in this paper, including an ultrasonic phased array and a 6-DOF cable-driven parallel mechanism (CDPM) with admittance control, which can be used to simultaneously stimuli kinesthetic and cutaneous receptors of humans.

The remainder of this article is organized as follows. In section II, the principles and mathematical models of ultrasonic array radiated force and CDPM kinematic are respectively presented, and the system architecture is also given. Section III details the rendering mechanism of our haptic device, which includes ultrasound tactile perception algorithm, rendering mechanism of cable-driven force feedback, and haptic synthesis methods. Section IV describes trials carried out on the prototype. We evaluate the cable-driven force system, and establish the regression model for tactile perception and the output pressure of the ultrasound phased array. We study the perception characteristics when multimodal haptic stimuli are simultaneously perceived, and validate the usefulness of prototype to increase perception and improve interaction. Section V discusses the results of the user study. Section VI relates our conclusions and proposes future work.

II. System Foundation and Architecture

The haptic feedback system is mainly composed of an ultrasonic tactile feedback device and a cable-driven parallel force feedback mechanism. In this section, we discuss the system foundation and architecture. The principles of the ultrasonic tactile system are discussed, the kinematic transformation of the cable robot model is proposed, and the hardware design of the prototype is presented.

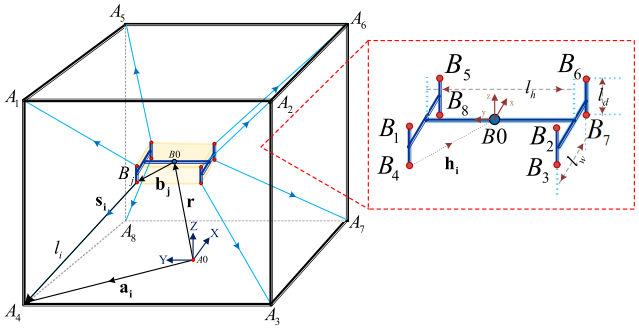

Fig. 1. Geometric and kinematic diagram of cable robot.

A. Ultrasound Tactile Principles

Acoustic radiation pressure is produced by a phased array composed of ultrasonic transducers, which are controlled individually with phase delays. Ultrasound focus generates pressure normal to the skin surface, which is strong enough to be noticed in the user's hand, and thus to induce a tactile sensation [23]. The algorithm to compute the sound pressure radiated from the phased array was proposed by Hoshi [10]. The single-frequency far-field piston model is calculated by the Rayleigh-Sommerfeld principle as

$$p(\Upsilon, \chi) = \Lambda P_{r0} \int_0^{b_m} \psi(\beta)\, e^{i\Lambda\chi\cos\beta} J_0(\Lambda\gamma \sin\beta) \sin\beta d\beta. \tag{1}$$

where $p(\Upsilon, \chi)$ is the distribution of the sound pressure, Υ and χ are the horizontal and vertical coordinates, respectively, near the focal point; Λ is the wavenumber; P_{r0} is the sound pressure at the intersection of the symmetry axis and the wavefront; b_m is the central angle of the central axisymmetric spherical wave; $\psi(\beta)$ is the sound pressure distribution function; and J_0 is the zero-order Bessel function.

B. Kinematic Model of Cable-Driven Apparatus

The CDPM we designed is a redundantly restrained positioning mechanism (RRPM) that has six DOF and it is inspired by [21], including eight cables, eight actuators, eight drivers, an end-effector, an CAN communication module, and a rectangular cubic frame. The geometric and kinematic diagram of the cable robot is presented in Fig. 1. A_i $(i = 1, 2, \ldots, 8)$ is defined as each actuator's position, B_j $(j = 1, 2, \ldots, 8)$ is the position of the distal anchor points on the end-effectors. The closure constraint for each cable can be written as

$$l_i \boldsymbol{s_i} = \boldsymbol{a_i} - \boldsymbol{r} - \boldsymbol{R}\boldsymbol{b_j}. \tag{2}$$

where l_i denotes the length of the cable i, $\boldsymbol{s_i}$ is the unit vector of cable i, and $\boldsymbol{r} = (x, y, z)^T$ is the position vector of the handle center. The position vector $\boldsymbol{a_i}$ denotes the proximal attachment points A_i on the frame in global coordinates $\{A0\}$. The vectors $\boldsymbol{b_j}$ denotes the distal attachment point B_j on the end-effector, which is given in motion coordinates $\{B0\}$. Rotation matrix $\boldsymbol{R}$ represents the orientation of the mobile platform, which can be obtained through the Rodrigues rotation formula.

The inverse and forward kinematics descriptions of CDPM are analyzed and obtained respectively. Inverse position kinematics is used to calculate the length of the cables from a

given pose of the end-effector, expressed as $(\boldsymbol{r}, \boldsymbol{R})$. Base on equation (2), the length of cable can be obtained as

$$l_i = [\boldsymbol{r}^T(\boldsymbol{r}) + \boldsymbol{b_j}^T(\boldsymbol{b_j}) + \boldsymbol{a_i}^T(\boldsymbol{a_i}) - 2\boldsymbol{r}^T(\boldsymbol{a_i}) + 2\boldsymbol{r}^T[\boldsymbol{R}(\boldsymbol{b_j})] - 2[\boldsymbol{R}(\boldsymbol{b_j})]^T(\boldsymbol{a_i})]^{1/2}. \quad (3)$$

Forward kinematics is used to calculate the end-effector's pose by the lengths of all cables, the length of each cable in equation (3) can derive seven nonlinear equations (4) as

$$\begin{cases} F_i(\boldsymbol{p_{os}}) = -l_i^2 + [\boldsymbol{a_i} - \boldsymbol{r} - \boldsymbol{R}\boldsymbol{b_j}]^T[\boldsymbol{a_i} - \boldsymbol{r} - \boldsymbol{R}\boldsymbol{b_j}], \\ f(\boldsymbol{p_{os}}) = \dfrac{1}{2}\sum_i F_i(\boldsymbol{p_{os}})^2. \end{cases} \quad (4)$$

where $\boldsymbol{p_{os}}$ is the end-effector's pose, expressed as $[x, y, z, \theta_x, \theta_y, \theta_z]^T$. In practical applications, compared to analytical solutions, numerical solutions are not sensitive to pose parameters, and can perform well when analytical solutions are degraded. Therefore, we use Gauss-Newton iterative method to solve $f(\boldsymbol{p_{os}}) = 0$ with a specified accuracy.

C. Prototype Specifications

To integrate multimodal stimulation modules, in terms of architecture and hardware design, the spatial layout as depicted in Fig. 2(a). 8 actuators are attached to the frame by the holder, each consisting of a planetary gearhead, DC motor, rotary encoder, pulley, and holder. Fig. 2(b) shows a photograph of the actuator. The DC motor (25 mm diameter, RE 25) is connected at the back of the gearhead (20 mm diameter, reduction gear ratio 1:4.4). The rotary encoder (500 pulses/round) is connected at the back of the motor. A pulley is attached to the same shaft in front of the motor. The diameter of the pulley is 20 mm, and the cable is wound inside the pulley. The other components of the CDPM are the drivers and communication module. The DC driver has a 12-bit D/A converter. A USB-CAN bus adapter is chosen to establish communication. The end-effector is a handle made of 3D printed resin. To minimize external disturbances on force measurement, force sensors are directly connected at the universal joints, which are attached to the distal anchor point of the handle, as shown in Fig. 2(c). The force sensor signals are amplified by the transmitter conditioner and sent to the DC motor driver, together with the pulses of the encoder and current value, and transferred to the computer.

Ultrahaptics STRATOS Explore Development Kit (USX) is used in this study, including 256 transducers (T4010A1), arranged in an area of $165 \times 165mm^2$. The time point streaming (TPS) API operating mode can give users direct control over the input parameters of intensity, position, modulation frequency, and waveform. Leapmotion is used to capture the hand pose, then the position information is transmitted to the ultrasonic phased array, enabling the tactile focus projected on the user's hand. A PC processes the data as a haptic interface server.

These devices are operated by applications created using LabVIEW, C++, Python, and Unity3D. The USX and cable robot can work independently or synchronously. A PC monitor displays the virtual environment established by Unity3D.

III. Rendering Mechanism of Haptic Device and Haptic Synthesis Method

In this section, the ultrasonic tactile rendering algorithm and the rendering mechanism of cable-driven force feedback are presented. Finally, two haptic synthesis methods are described.

A. Midair Ultrasonic Tactile Rendering

A new ultrasonic tactile perception model is developed to ensure precise control of the user's ultrasonic tactile feedback. The modulation waveform is introduced into the control process of ultrasonic tactile perceived magnitude as an input parameter, to improve the tactile rendering effect.

Research of ultrasonic tactile perceived strength has focused on influence factors such as the position of focus, frequency, and command intensity, ignoring the modulation waveform effect [24]. Modulation waveforms were found to have an impact on the output pressure of the focus, and a mapping regression model for input parameters and output pressure was established [25]. The relationship between input command intensity and output pressure at different frequencies is established as

$$OP_\iota = Q_\iota I^{\varrho_1} + N_\iota I^{\varrho_1 - 1} + \cdots + T_\iota, \quad (5)$$

where OP_ι is defined as the output pressure, and its unit is gf (gram force), ι is the corresponding frequency, ranging from 80 to 300 Hz; I is the input command intensity, it is a unit-less floating-point number from 0 to 1; and Q_ι, N_ι, and T_ι are the coefficients of the polynomial for different modulation frequencies. The relationship between the distance from the center axis and output pressure pl_{max} at a certain height is described by

$$pl_{max}(d) = Cp_{\varrho_2} d^{\varrho_2} + Cp_{\varrho_2 - 1} d^{\varrho_2 - 1} + \cdots + Cp_0, \quad (6)$$

where d is the distance from the focus to the center axis (mm); and Cp_{ϱ_2}, $Cp_{\varrho_2 - 1}$, $\cdots$, Cp_0 are polynomial coefficients. The model used to fit the output pressure H_{max} at different positions along the z-axis is

$$H_{max}(h) = Pz_{\varrho_3} h^{\varrho_3} + Pz_{\varrho_3 - 1} h^{\varrho_3 - 1} + \cdots + Pz_0, \quad (7)$$

where h is the distance from the array to the focus (mm); and Pz_{ϱ_3}, $Pz_{\varrho_3 - 1}$, $\cdots$, Pz_0 are polynomial coefficients. This model is used to fit the output pressure H_{max} at different positions along z-axis direction.

In addition to the above impact factors, we introduce the modulation waveform as an input parameter for the perceived magnitude model. The effect of the modulation waveform on the output pressure O_{wf} is

$$O_{wf} = F_{wf} O_{sq}, \quad (8)$$

where F_{wf} is the coefficient of waveform wf, and O_{sq} is the output pressure of the square waveform, which is greater than that of waveforms absolute value of sine, sine, sawtooth, cosine, and triangle. As the duty cycle of the square waveform increases, the output pressure increases, displaying a linear relationship,

$$O_{sq}(Rd) = S_{fo} Rd + S_{ct}, \quad (9)$$

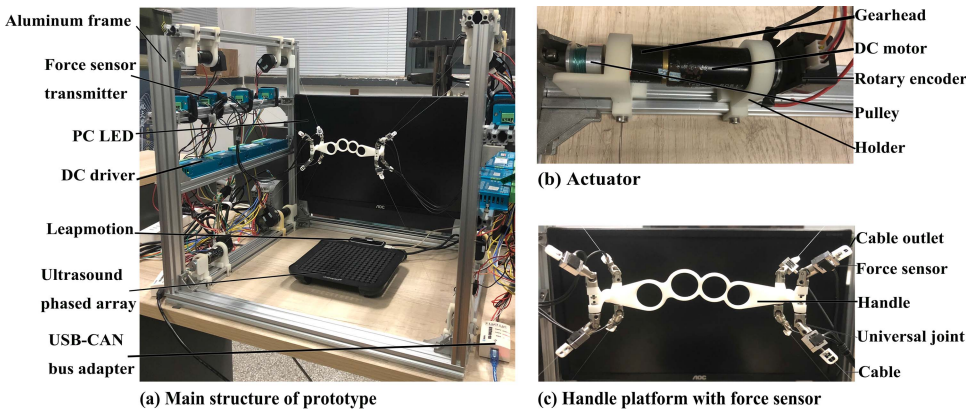

Fig. 2. Setup of haptic interface device.

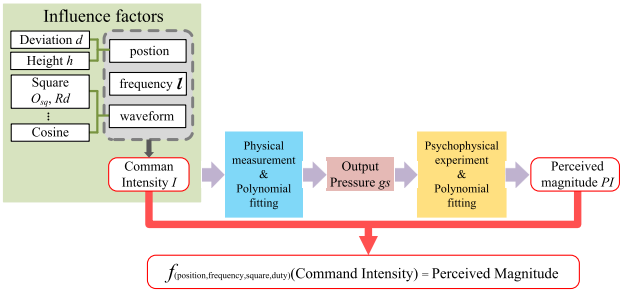

Fig. 3. Framework diagram: mapping from command intensity to perceived magnitude.

where Rd is the duty ratio of the square wave, S_{fo} and S_{ct} are linear coefficients. Previous studies have typically used the cosine wave as a modulation waveform because it can produce strong tactile points without loud noise disturbance. The square wave was selected for three reasons: (1) the tactile rendering effect is further guaranteed because a square wave can generate greater output pressure than a cosine waveform; (2) a good linear relationship between the duty cycle of the square wave and corresponding output pressure makes the perceived magnitude easier to control accurately; (3) users need to wear headphones with white noise to block out acoustic disturbances. Hence, we can ignore the influence of the noise factor on waveform selection.

The relation between the perceived magnitude and the pressure value of the focus is assumed as a polynomial model,

$$PI_\iota = G_\iota gs^{\varrho 4} + J_\iota gs^{\varrho 4-1} + \cdots + V_\iota, \tag{10}$$

where PI_ι is the perceived magnitude, it is a unit-less positive number that can be obtained through a series of psychophysical experiments described in Section IV; gs represents the output pressure value; and G_ι, J_ι, and V_ι are the coefficients of the polynomial model. Combining equation (10) with the physical model described by (5)-(9), the route from input command intensity to perceived magnitude is constructed, as shown in Fig. 3.

After the perceived magnitude is determined by the haptic interface designers, the pressure value can be derived by the inverse of (10), and it is later modified by the scaling factor of the impact parameters. This gf value can be directly inserted into the inverse of (5),

$$\begin{cases} I_{gF} = L_\iota gF^{\varrho 5} + M_\iota gF^{\varrho 5-1} + K_\iota gF^{\varrho 5-2} + \cdots + U_\iota, \\ gF = gsF_I. \end{cases} \tag{11}$$

to yield the input command intensity, where I_{gF} is the desired intensity; L_ι, M_ι, K_ι, and U_ι are the coefficients of the polynomial for different frequencies; gF is the modified gs which is normalized by the effect of height, waveform, lateral deviation, and square wave duty ratio; and

$$F_I = F_{pl}F_H F_D F_{wf}^{-1}, \tag{12}$$

where F_{pl}, F_H, F_{wf}, and F_D are the impact factors of the distance from the center, height, waveform, and duty of the square waveform, respectively, calculated as

$$\begin{cases} F_{pl} = pl_{max}(d_{max})/pl_{max}(d), \\ F_H = H_{max}(h_{max})/H_{max}(h), \\ F_D = O_{sq}(Rd_{max})/O_{sq}(Rd). \end{cases} \tag{13}$$

where $pl_{max}(d_{max})$, $H_{max}(h_{max})$, and $O_{sq}(Rd_{max})$ are the maximum output pressure values of $pl_{max}(d)$, $H_{max}(h)$, and $O_{sq}(Rd)$, respectively, which can be obtained from (6), (7) and (9). For richer and more accurate tactile information, a model of ultrasonic tactile perception is developed, as mentioned above, which can be used to dynamically control the perceived magnitude. Ultrahaptics can project 3D volume shapes above the phased array, it is generally used to render the outline, boundary, and shape of virtual objects [26]. The best-perceived area of ultrasonic tactile is between 10 cm and 50 cm above the array surface.

B. Rendering Mechanism of Cable-Driven Force Feedback

One key problem in the control of CDPM is the distribution of the external forces and torques acting on the end-effector to the cables. The cable force distribution algorithm is used to control the force distribution on each cable to achieve the force feedback required on the end-effector. The structure equation

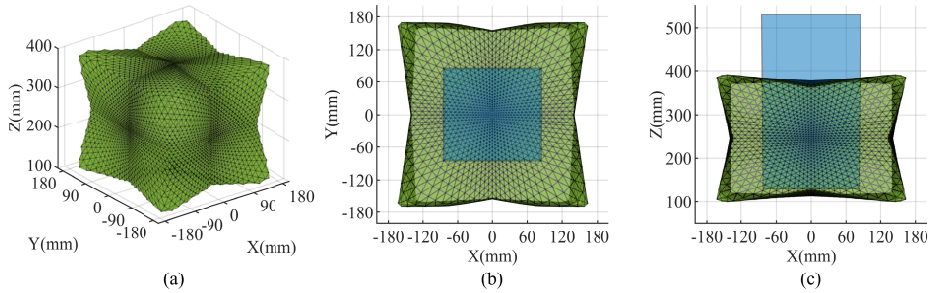

Fig. 4. Useful workspace of our system: (a) 3D representation of useful workspace (±15°) for cable robot; (b) vertical view of useful workspace for our haptic device (blue area represents USX workspace); (c) side view of useful workspace for our haptic device.

can be expressed as

$$\begin{cases} \boldsymbol{f_H} = \boldsymbol{s_1}t_1 + \boldsymbol{s_2}t_2 + \boldsymbol{s_3}t_3 + \boldsymbol{s_4}t_4 + \boldsymbol{s_5}t_5 + \boldsymbol{s_6}t_6 \\ \quad + \boldsymbol{s_7}t_7 + \boldsymbol{s_8}t_8, \\ \boldsymbol{t_H} = (\boldsymbol{s_1} \times \boldsymbol{h_1})t_1 + (\boldsymbol{s_2} \times \boldsymbol{h_2})t_2 + (\boldsymbol{s_3} \times \boldsymbol{h_3})t_3 \\ \quad + (\boldsymbol{s_4} \times \boldsymbol{h_4})t_4 + (\boldsymbol{s_5} \times \boldsymbol{h_5})t_5 + (\boldsymbol{s_6} \times \boldsymbol{h_6})t_6 \\ \quad + (\boldsymbol{s_7} \times \boldsymbol{h_7})t_7 + (\boldsymbol{s_8} \times \boldsymbol{h_8})t_8. \end{cases} \tag{14}$$

where t_i is the tensions on active cable l_i, the orientation of $\boldsymbol{s_i}$ is described in Fig. 1, $\boldsymbol{h_i}$ is a vector from the handle attachment point B_j to the center of the handle, $\boldsymbol{f_H}$ is the sum of forces on the handle, and $\boldsymbol{t_H}$ is the sum of moments acting on the handle. This equation is used to determine how much tension to apply on the actuated cables. Equation (14) can be written in matrix form as

$$\underbrace{\begin{bmatrix} \boldsymbol{s_1} & \cdots & \boldsymbol{s_i} \\ \boldsymbol{s_1} \times \boldsymbol{h_1} & \cdots & \boldsymbol{s_i} \times \boldsymbol{h_i} \end{bmatrix}}_{\boldsymbol{A^T}} \underbrace{\begin{bmatrix} t_1 \\ \vdots \\ t_i \end{bmatrix}}_{\boldsymbol{t}} = -\underbrace{\begin{bmatrix} \boldsymbol{f_H} \\ \boldsymbol{t_H} \end{bmatrix}}_{\boldsymbol{W}}. \tag{15}$$

where $\boldsymbol{A}^T$ is the transpose of the Jacobian matrix, and $\boldsymbol{t}$ is the cable force vector, also called the cable force distribution. The optimal set of cable tensions can be found as

$$\begin{cases} \boldsymbol{t} = \zeta \boldsymbol{t}_g + \boldsymbol{t}_s, \\ \zeta = \max\limits_{i=1,\ldots,8} ((\boldsymbol{t}_{min} - \boldsymbol{t}_{s_i})/\boldsymbol{t}_{g_i}). \end{cases} \tag{16}$$

where $\boldsymbol{t}_g$ can be caculated from the relation $\boldsymbol{A}^T\boldsymbol{t}_g = \boldsymbol{0}$. A particular solution, $\boldsymbol{t}_s = \boldsymbol{A}^{T+}\boldsymbol{t}$, can be solved by the Moore-Penrose pseudo-inverse. To straighten the strings and overcome the friction of the fulcrum, pulley, and cables, the minimum force $\boldsymbol{t}_{min}$ on the cable is set to 0.5 N. Based on application and security considerations, the maximum force $\boldsymbol{t}_{max}$ is set to 10 N.

The workspace of a CDPM is an important property to realize the haptic fusion of cable-driven force and ultrasonic tactile feedback. The most important criterion to decide if a pose belongs to the cable robot workspace is whether the platform can be statically balanced through positive tension on the cables. The boundary of the workspace is represented by its hull triangulation [21].

In practice, cable length and interference between cables need to be fully considered. In our device, the length of each cable is kept between 32 mm and 486 mm. The volume of the useful workspace, ±15° for orientations θ_x, θ_y, and θ_z, is $7.518\times10^6 mm^3$, and its 3D representation is shown in Fig. 4(a). The green area in Fig. 4(b) and (c) is the useful workspace of the cable robot, the blue area is the workspace of USX, and their intersection is the useful workspace of the prototype.

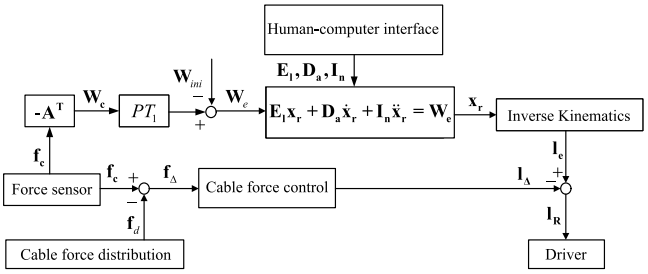

Fig. 5. Force rendering control structure of cable-driven parallel mechanism.

In our work, admittance control method is introduced to improve the effect of interaction control between CDPM and operator. The input of the admittance control is the actual applied force, and the output corresponds to the end-effector position. The six-dimensional spring-mass-damper (SMD) system model is represented as

$$\boldsymbol{I_n}\ddot{\boldsymbol{x}}_{\boldsymbol{r}} + \boldsymbol{D_a}\dot{\boldsymbol{x}}_{\boldsymbol{r}} + \boldsymbol{E_l}\boldsymbol{x_r} = \boldsymbol{W_e}. \tag{17}$$

where $\boldsymbol{W_e} \in \boldsymbol{R}^{6\times1}$ is the external force and torque applied to the object, i.e., the force wrench. The desired pose is $\boldsymbol{x_r}$ and its time derivatives are $\dot{\boldsymbol{x}}_{\boldsymbol{r}}$ and $\ddot{\boldsymbol{x}}_{\boldsymbol{r}}$. Diagonal matrices $\boldsymbol{I_n}$, $\boldsymbol{D_a}$ and $\boldsymbol{E_l}$ is Inertia, damping, and stiffness coefficient, respectively. Based on the cable force measurement and kinetic model described above, the control structure of the cable parallel robot is depicted in Fig. 5.

The wrench $\boldsymbol{W_c}$ is derived by $\boldsymbol{W_c}$=$-\boldsymbol{A}^T\boldsymbol{f_c}$, where the $\boldsymbol{f_c}$ is the tension on the cable, which can be measured by the force sensor attached to the handle. Gravitational force, inertia forces, and measurement errors should be excluded from $\boldsymbol{W_c}$. Mathematically, the input signal of the admittance controls $\boldsymbol{W_e}$ yields

$$\begin{cases} \boldsymbol{W_e} = \boldsymbol{W_c} - \boldsymbol{W_{ini}}, \\ \boldsymbol{W_{ini}} = m_e\ddot{\boldsymbol{x}}_{\boldsymbol{r}} + m_e\boldsymbol{g}. \end{cases} \tag{18}$$

where m_e is the end-effector mass. According to equation (4), the desired length of each cable $\boldsymbol{l_e}$ can be calculated from the desired pose $\boldsymbol{x_r}$ through inverse kinematics.

The desired cable force distribution $\boldsymbol{f_d}$ is calculated by equation (16). A cable force algorithm [27] is used to keep the cables under tension while employing the admittance control. Thus the change in cable length $\boldsymbol{l_\Delta}$ can be obtained through

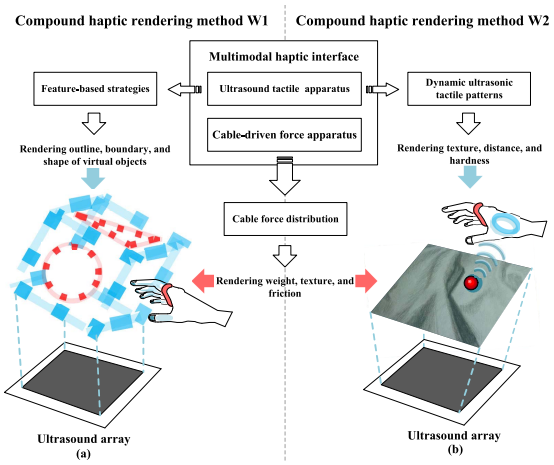

Fig. 6. Schematic diagram of haptic synthesis method: (a) users explore shapes and textures of virtual objects rendered by multimodal systems; (b) moving an object on a wrinkled desktop.

the cable force controller. The output of the cable-driven force apparatus controller is

$$\boldsymbol{l_R} = \boldsymbol{l_e} - \boldsymbol{l_\Delta}. \tag{19}$$

where $\boldsymbol{l_R}$ is the cable length variable transmitted to the servo drivers.

C. Haptic Synthesis Method

When integrating multimodal stimulus modules, in addition to the structure and hardware design, multimodal fusion methods must be considered [28]. Multiple stimuli can be exerted in a collocated way on the user's skin in the workspace. The hand is the most sensitive region available for ultrasound tactile stimulation, and is the best area for studying human ultrasonic tactile perception [29]. The cable-driven force is applied to the handle, and the force stimulation is transmitted to the hand through the handle. The cable-driven force mainly acts on the hand joints through the handle, and the ultrasonic tactile mainly acts on the fingertips and palm, there is no interference between stimulation areas. In our work, force stimulation of CDPM is used to render the weight, texture, and friction of virtual objects, which is expected to compensate for the intensity and spatial resolution of ultrasonic tactile feedback. Based on the different working modes of ultrasonic tactile, two compound haptic rendering methods are investigated (see Fig. 6), labeled W1 and W2, respectively, making full use of the advantages of ultrasonic tactile, both kinesthetic and tactile sensations are invoked simultaneously.

In the rendering mode W1, users can perceive virtual objects (volume, size, and shape) through the feature-based strategies of multi ultrasonic tactile points [30]. Taking the rendering schematic of Fig. 6(a) as an example, the vertex and edge information units are marked in blue cubes, which are rendered by ultrasound tactile. If the edge and vertices collide with the hand module slice plane (captured by Leapmotion), the collision points are represented by ultrasonic tactile. Each red cube represents a cell of texture on an object's surface, which is rendered by cable-driven force. Users can quickly identify multiple features of an object. This method is useful when users explore a model in the virtual environment.

In the rendering mode W2, the feature information (texture, distance, hardness) in the virtual environment is delivered by dynamic ultrasonic tactile patterns projected on the palm, such as varied tactile intensities, pulse frequencies (vibration frequencies), and transformations (translation, rotation, and scaling). Fig. 6(b) shows an example of the W2 rendering method, in which a user moves an object on the desktop in the virtual environment, and the gravity information can be obtained through the cable-driven force feedback. The texture information of the tablecloth is transmitted to the user by an ultrasonic tactile ring with different vibration frequencies. This method is useful when users complete operational tasks in the virtual environment.

This is the first study on the integrated rendering method of cable-driven force and ultrasonic tactile. According to the above methods, the prototype can produce multimodal haptic stimuli, which can be used in complex human-computer interaction tasks. Our haptic device has full potential to be deeply explored, because of the non-contact property of ultrasonic tactile feedback in midair and the cable parallel robot's good expansibility.

IV. User Study

A. Objectives

In this section, the trials carried out on our haptic system are described. The user study included four tasks as T1-T4. Task T1 was designed to evaluate the cable-driven force feedback system. Task T2 was conducted to establish the perceived magnitude model of ultrasonic tactile. The purpose of task T3 was to study the perception characteristics when cable-driven force and ultrasonic tactile stimuli were being perceived simultaneously. Task T4 was designed to evaluate our multimode haptics system, and to analyze the effect of compound haptics rendering methods.

B. Experimental Design and Setup

In task T1, a virtual workspace was introduced, in which the elements of the stiffness matrix were a function $\boldsymbol{S_{ti}} = f(\boldsymbol{x_r})$ of the pose, which limited the reachable workspace by applying a virtual spring force at the border. The virtual workspace was divided into three zones. Z1 was a sphere with radius 40 mm, located in the center of the haptic workspace. The ball center was the static pose point for the handle. No matter where the handle was located in this area, the spring force vector could pull it to the origin. In Z2, no spring force was rendered; only the damping and inertia of the virtual system were activated. The radius was 120 mm. If no force was applied on the handle, it would slow to the static state. In Z3, the radius was 160 mm, and subjects could feel spring force while grasping the handle, which could guide the end-effector to Z2. The spring force vector pointed to the origin of the workspace. Subjects moved handle to several positions at their will. Through experiments, we found that the update rate of the CDPM handle is 33.3 Hz. The applied wrench in the z-direction, w_z, and the resulting movement in the z-direction, $x_{r,z}$, were recorded. Three subjects took part in T1, of age 30, 32, and 34 respectively, all right-handed. The experiment was carried out on the cable-driven force feedback system.

TABLE I
POLYNOMIAL COEFFICIENTS FOR EQUATION (11)

$\iota[Hz]$	L_ι	M_ι	N_ι	U_ι	R_ι^2
80	2.079	-3.131	2.411	0.2146	0.99
100	2.806	-3.849	2.614	0.2308	0.96
140	3.282	-4.2805	2.7235	0.2422	0.94
180	3.744	-4.675	2.791	0.2585	0.92
240	4.312	-5.127	2.888	0.2697	0.98
300	5.454	-6.006	3.105	0.2759	0.99

Task T2 was carried out on USX, to establish the mapping regression model from output pressure intensity to the perceived magnitude of the ultrasonic tactile focus, the modulation waveform was a square wave. The focal point was on the center axis, 200 mm from the array. The modulation waveform was a square wave with duty ratio 50%. The experiment consisted of 48 conditions—combinations of six modulation frequencies (80, 100, 140, 180, 240, and 300 Hz) and eight out pressure values (gf)—associated with the corresponding input intensity commands. The mapping relationship from the gf value to input command intensity is described by equation (11), where values of coefficients for each frequency are reported in Table I. The patterns were presented in random order. Stimuli were rendered at the participant's palm. The experiment used absolute magnitude estimation [31]. Participants were asked to rate the perceived magnitude of the stimulus on a free scale (zero responses were not considered). Each condition was performed twice. Sixteen subjects (six females and 10 males, age from 25 to 35, all right-handed) took part in T2. The arm was placed on the armrest, and the palm faced the USX. To minimize fatigue, participants were given five seconds to rest after each stimulus, and 45 seconds after every five minutes.

In task T3, the absolute detection thresholds of ultrasonic tactile on the finger and palm under cable-driven force stimuli were measured, to study the perception characteristics when two modalities of stimuli were being perceived simultaneously. A focal point 200 mm from the array surface on the central axis was rendered while varying force feedback, tactile input intensity, and frequency. The modulation waveform was a square wave (50% duty ratio). This task was divided into two groups. In the first group, stimuli were projected on the participant's palm in two conditions: (1) the bare hand, where subjects were presented with a randomized sequence of a focal point with rendering frequencies of 80, 100, 140, 180, 240, and 300 Hz; and (2) wearing the handle, where, in addition to the difference in modulation frequency, force feedback had values of 1, 3, 6, and 10 N. Hence each sequence included 24 rendering methods for the presentation of a pattern in random order. The second group used the same experimental stimuli as in the first group, projected on the index fingertip. The adaptive method with staircase procedures was used in this task. The input command intensity was set from 0 to 1 in an ascending series, and from 1 to 0 in a descending series. To avoid errors of expectation, in each trial, one of the two sequences was randomly selected with an equal a priori probability of 0.5. In staircase procedures, subjects were asked whether they felt a stimulus, and responses were recorded at each level. The trial of each sequence stopped once eight reversals had occurred. To increase the precision in estimating the threshold, a larger step size (3 dB) was used for the first three reversals, and smaller step size (1 dB) was used for the remaining reversals. The first three reversals were not considered in the data analysis. The remaining five were averaged to obtain an estimate of the absolute detection threshold. To avoid a learning effect due to task 2, another set of 12 subjects (five females and seven males, aged from 25 to 35, all right-handed) took part in task 3. All subjects perceived a haptic point rendered with ultrasonic tactile and cable-driven force stimuli to the index finger or palm. The experimental interval rest times were the same as for task 2.

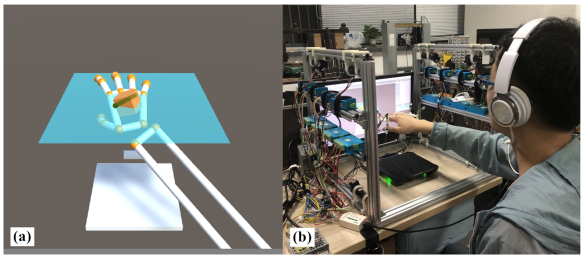

Fig. 7. Overview of T4 experimental setup.(a) A virtual environment in Task 4 (screenshot). (b) A participant trying to move an object to a given height in Task 4.

In task T4, participants were asked to place a virtual cube at a height of 25 cm. Once a participant determined that the target height had been reached, the actual height of the cube and the time to perform the process were recorded. T4 included experiments $G1_{w1}$, $G2_{w2}$, and $G3_{w2}$, presented in random order for each subject. The weight sensation of the cube was rendered by cable-driven force feedback, which was set at 1 N. In $G1_{w1}$, using W1 as the haptic synthesis method, a virtual plane was set at a distance of 25 cm from the USX surface, which was rendered by ultrasonic tactile. Subjects moved the object above the plane, then placed the cube. The line segments of hand-plane intersections were processed into focus points, and the perceptual magnitude of each point was set at the same value. $G2_{w2}$ and $G3_{w2}$ used method W2, and the ultrasonic focus was projected on the palm. $G2_{w2}$ used vibration patterns; as the cube approached the desired height, the vibration frequency of the ultrasonic tactile stimuli increased. $G3_{w2}$ used perception intensity mode; as the cube approached the desired height, the ultrasonic tactile intensity perceived by the palm increased. Nine subjects (three females and six males, age from 25 to 35, all right-handed) took part in T4. The experiments were carried on our multimodal haptics system (Fig. 7). Subjects could rest for 60 seconds after each experiment.

All subjects used USX, and wore headphones that played white noise to avoid the potential effects of ultrasound noise cues. They were asked to experience a short demonstration (virtual ball rendering by USX demo suite) to familiarize themselves with ultrasonic tactile sensation before starting the experiment.

V. EXPERIMENTAL RESULTS

The experiment results are summarized as follows.

In task 1, the participant moved the hand with the handle up and down to explore the virtual workspace. We take the test result of participant 1 as an example, which is plotted in

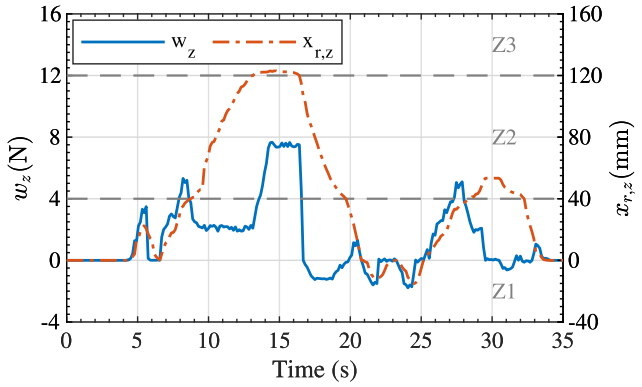

Fig. 8. Measured user-applied force w_z and resulting position $x_{r,z}$.

TABLE II
PALM PERCEPTIVE MAGNITUDE MODEL COEFFICIENTS

$\iota[Hz]$	G_ι	J_ι	V_ι	R^2_ι
80	-10.39	23.17	-0.2071	0.97
100	-20.49	27.86	-0.3396	0.96
140	-16.59	23.47	0.1361	0.96
180	-12.46	20.88	-0.1070	0.95
240	-9.518	12.93	0.1897	0.96
300	-3.682	6.118	0.3376	0.99

Fig. 8. The first force applied could not bring the handle out of Z1; then the handle was dragged back to the origin by spring force. The next force was strong enough to bring the handle to Z2, where there was no spring force. The slope of position $x_{r,z}$ increased when there was no effect of stiffness, and led to a drop of applied force w_z. Then the slope of the position maintained a constant value while the applied force stayed in a constant range. This showed the damping in Z2. The w_z value rose with a small delay after the handle reached the border of Z2 and Z3, due to the virtual inertia of the system. Due to that, the handle entered Z3 without additional force from the user. As it was visible, the user pressed the handle to Z3 by constant force. The position of the handle did not change because the spring force of Z3 equaled the force applied by the user. After the user released the force, the handle moved back to Z2. The user felt a guiding force toward the border plane between Z3 and Z2. Back to Z2, the handle moved to the negative direction of the Z-axis. The next two force pulses were not strong enough to bring the handle out of Z1, and the handle was dragged back to the origin by spring force. After that, the applied force was strong enough to bring the handle to Z2. The user's feeling at this point was comparable to the impression of dragging two magnets apart. Later, the handle was dragged back to the Z1 border plane. Finally, the spring force of the Z1 caught the platform and dragged it to the origin. Fig. 8 shows $x_{r,z}$ was very responsive to user input, and system behavior could be controlled precisely.

In task 2, the recorded data were normalized separately [32]. The normalization factor can be determined as the ratio of the average of individual geometric means for each waveform to individual geometric means. The perception magnitude was the product of a subject's response and the corresponding normalization factor. The horizontal axis of the graph in Fig. 9 is the output pressure (gf), and the corresponding input command intensity is calculated by equation (11). The vertical axis is the perceived magnitude. In each graph, the error bars

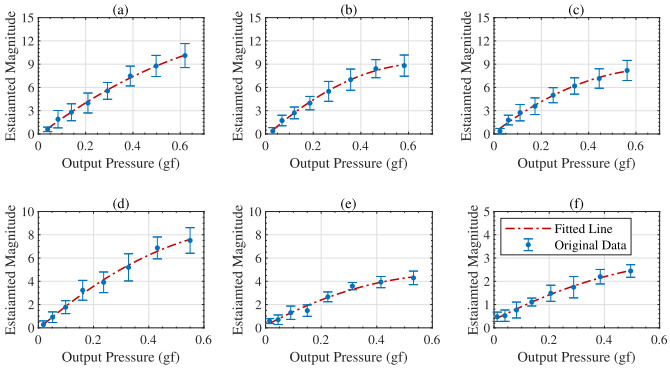

Fig. 9. Measured perceived magnitude for each waveform on palm. (a) 80Hz. (b) 100Hz. (c) 140Hz. (d) 180Hz. (e) 240Hz. (f) 300Hz.

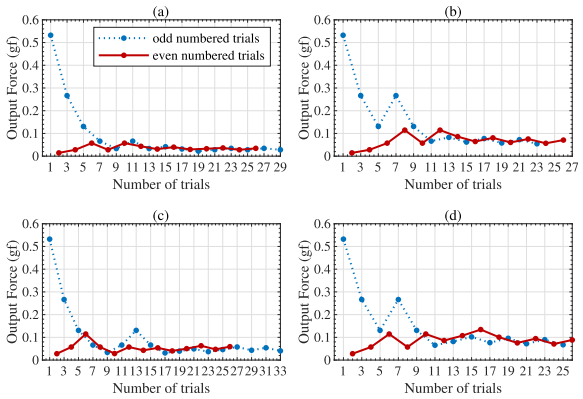

Fig. 10. Results of T3. (a) 240 Hz, bare hand, stimuli palm; (b) 240 Hz, handle with 1 N force feedback, stimuli palm; (c) 240 Hz, bare hand, stimuli index finger; (d) 240 Hz, handle with 1 N force feedback, stimuli index finger.

in blue show the standard deviation. The relationship between perceived magnitude and output pressure can be modeled using the second-order polynomial model (10), illustrated by a red dashed line in Fig. 9. The values of the coefficients for the palm perceptive magnitude model are reported in Table II.

In task 3, our study focused on the absolute threshold (AL) of ultrasonic perception under two compound haptics rendering methods. Fig. 10 shows the results of the first (stimuli at fingertip) and second (stimuli at palm) experiment groups, there were two different starting points of the staircase procedure, odd-numbered trials begin with the high-intensity command, even-numbered trials begin with the perceptually low stimulus. Table III lists the minimum perceivable ultrasonic tactile for finger and palm under different force stimuli F_{al}. These results can be used to modify the definition domain of the input variable gs in (11), and to optimize the ultrasonic tactile perceivable strength algorithm used in our multimodal rendering. The minimum perceivable ultrasonic tactile threshold increased with the cable-driven force stimuli. However, when the AL reached around 0.1 gf, even if the force stimuli increased, the minimum ultrasonic perception threshold would not change significantly. This indicates that when the output pressure of the ultrasonic focus increases to a certain value, the influence of the cable-driven force stimulation on ultrasonic tactile perception gradually weakens. The interaction of the two modalities would not affect the user's haptic feedback experience while using the multimodal haptic device.

TABLE III
AL ULTRASOUND TACTILE FOR FINGER AND PALM UNDER DIFFERENT FORCE FEEDBACK

$F_{al}[N]$	AL tactile for finger$[gf]$	AL tactile for palm $[gf]$
1	$(0.06568, 0.09169)$	$(0.05903, 0.06903)$
3	$(0.08252, 0.1005)$	$(0.06794, 0.08392)$
6	$(0.08701, 0.1053)$	$(0.07794, 0.0946)$
10	$(0.1094, 0.1161)$	$(0.09028, 0.1042)$

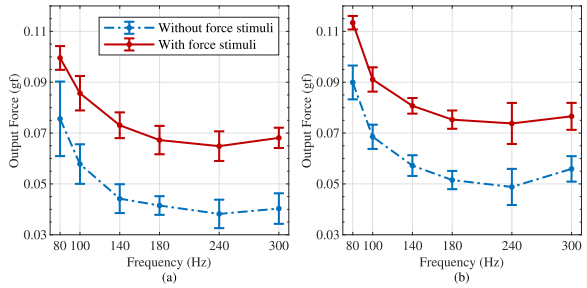

Fig. 11. The minimum perceivable ultrasonic tactile values for all frequencies. (a) palm. (b) index finger.

TABLE IV
OFFSET IN MILLIMETERS BETWEEN THE DESIRED HEIGHT AND THE FINAL HEIGHT DETERMINED BY THE USER

	$U1$	$U2$	$U3$	$U4$	$U5$	$U6$	$U7$	$U8$	$U9$	abs. Avg
G_{w1}	14	24	15	7	10	15	9	-9	-10	12.6
G_{w2}	7	11	8	5	5	9	-5	4	4	6.4
G_{w3}	6	8	6	1	3	5	-4	2	4	4.3

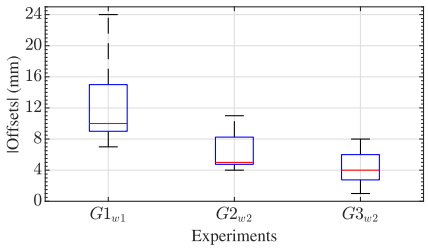

Fig. 12. Absolute value of error between the target heights and final values.

Fig. 11 shows the minimum perceivable ultrasonic tactile of palm and finger for all frequencies under two conditions (with or without cable-driven force stimuli). It reveals that whether or not there is cable-driven force stimuli, the most sensitive frequency band for fingertip and palm is 180-240 Hz. Compared with the bare hand, the minimum perceivable ultrasonic tactile increased under the cable-driven force stimuli. The ultrasonic tactile perception of the palm is more sensitive than that of the finger. This indicates that in a virtual environment rendered by ultrasonic tactile, the finger is more suitable to explore and determine the boundary characteristics of virtual objects, while the palm is suitable for sensing different degrees of ultrasonic tactile stimulation. The physical characteristics of the virtual object can be rendered by different forms, such as vibration frequencies and output pressure intensities. It is the basis of the two compound rendering methods we designed.

In task 4, subjects were asked to rate whether the ultrasound tactile feedback helped their manipulation. Aggregate results show the average rating 3.77 ($G1_{w1}$, σ: 0.85), 3.45 ($G2_{w2}$, σ: 1.01), and 3.51 ($G3_{w2}$, σ: 1.03), with 1 indicating not helpful, and 5 very helpful. Most users said they could identify the right position by means of multiple modal haptics feedback. The intuitiveness of the task process were labeled as 4.02 on average ($G1_{w1}$, σ: 1.14), a 3.25 ($G2_{w2}$, σ: 1.02), and a 3.63 ($G3_{w2}$, σ: 1.11), 1 is not intuitive at all, and 5 is very intuitive. Some 48.6% of the users said manipulation progress was more intuitive while using G_{w1} mode, 17.3% answered $G2_{w2}$, 25.5% answered $G3_{w2}$, and the remaining 8.6% said there was no significant difference. This shows that the W1 method is more suitable to the task of exploring virtual environments and determining boundary characteristics. When rating how difficult it was to reach the exact height (1 is not difficult at all; 5 is very difficult), 2.31 on average, σ: 1.83. The fact is that some users confuse and misjudge the position of the object when their hands pass across the ultrasonic tactile plane, due to the different perception magnitudes of ultrasonic tactile stimuli on fingertips and palms. Table IV shows the experimental results of nine human subjects, including the offset between the target height and the final value, as well as the absolute average value (mm) under different rendering methods. Fig. 12 shows the absolute value of offsets between the target heights and final values (mm). A one-way ANOVA shows a significant difference with respect to the accuracy achieved among the three rendering modalities ($F(2, 24)$=13.11, p=0.0001); the deviation results of $G1_{w1}$ were greater than $G2_{w2}$ and $G3_{w2}$. Multiple comparisons did not show a significant difference of the means of groups $G2_{w2}$ and $G3_{w2}$. The time for task completion was not significantly different between compound rendering methods ($F(2, 24)$=0.43, p=0.265). Therefore, the multimodal haptics used in our system can help us manipulate virtual objects more accurately, especially the W2 haptic synthesis method.

VI. CONCLUSION AND FUTURE WORK

In this paper, a novel multimodal haptic sensor system is presented. The prototype included an ultrasonic tactile feedback system and 6-DOF cable-driven parallel robot with admittance control. It could provide compound stimuli to simultaneously invoke both kinesthetic and tactile sensation.

To enhance the rendering effects of each subsystem, an admittance control was developed for the cable-driven force feedback. Experimental results showed that the manipulation of the end-effector can be controlled precisely. Compared with related works, the modulation waveform is first introduced into the perceived strength model as the control variable, the relationship between ultrasonic output pressure and human skin perception is explored. To invoke realistic compound haptic sensations, the perceived characteristics of multimodal haptic stimuli were investigated by absolute detection threshold experiments, and compound rendering methods were designed to combine cable-driven force and ultrasonic tactile stimulations. A series of experiments showed that users can manipulate a virtual object more accurately when using our system.

In the future, we will consider integrating more haptic devices (such as AR, Laser Haptics, or wristbands) into our system, while enriching the perceived sensations in immersive virtual environments and extending the range of perceptions.

REFERENCES

[1] S. J. Lederman and R. L. Klatzky, "Haptic perception: A tutorial," *Attention, Perception, Psychophys.*, vol. 71, no. 7, pp. 1439–1459, 2009.

[2] S. Gallo, L. Santos-Carreras, G. Rognini, M. Hara, A. Yamamoto, and T. Higuchi, "Towards multimodal haptics for teleoperation: Design of a tactile thermal display," in *Proc. 12th IEEE Int. Workshop Adv. Motion Control (AMC)*, Sarajevo, Bosnia and Herzegovina, Mar. 2012, pp. 1–5.
[3] E. Whitmire, H. Benko, C. Holz, E. Ofek, and M. Sinclair, "Haptic revolver: Touch, shear, texture, and shape rendering on a reconfigurable virtual reality controller," in *Proc. CHI Conf. Hum. Factors Comput. Syst.*, Montreal, QC, Canada, Apr. 2018, pp. 1–12.
[4] Y. Wang, Y. Lu, D. Mei, and L. Zhu, "Liquid metal-based wearable tactile sensor for both temperature and contact force sensing," *IEEE Sensors J.*, vol. 21, no. 2, pp. 1694–1703, Jan. 2021.
[5] Y. Yang, Y. Zhang, B. Lemaire-Semail, and X. Dai, "Enhancing the simulation of boundaries by coupling tactile and kinesthetic feedback," in *Proc. 9th Int. Conf. EuroHaptics*, Versailles, France, Jun. 2014, pp. 19–26.
[6] P. Puangmali, K. Althoefer, L. D. Seneviratne, D. Murphy, and P. Dasgupta, "State-of-the-art in force and tactile sensing for minimally invasive surgery," *IEEE Sensors J.*, vol. 8, no. 4, pp. 371–381, Apr. 2008.
[7] S. Denei, P. Maiolino, E. Baglini, and G. Cannata, "Development of an integrated tactile sensor system for clothes manipulation and classification using industrial grippers," *IEEE Sensors J.*, vol. 17, no. 19, pp. 6385–6396, Oct. 2017.
[8] D. Wang, K. Ohnishi, and W. Xu, "Multimodal haptic display for virtual reality: A survey," *IEEE Trans. Ind. Electron.*, vol. 67, no. 1, pp. 610–623, Jan. 2020.
[9] L. R. Gavrilov, G. V. Gersuni, O. B. Ilyinski, E. M. Tsirulnikov, and E. E. Shchekanov, "A study of reception with the use of focused ultrasound. I. Effects on the skin and deep receptor structures in man," *Brain Res.*, vol. 135, no. 2, pp. 265–277, Oct. 1977.
[10] T. Hoshi, M. Takahashi, T. Iwamoto, and H. Shinoda, "Noncontact tactile display based on radiation pressure of airborne ultrasound," *IEEE Trans. Haptics*, vol. 3, no. 3, pp. 155–165, Jul./Sep. 2010.
[11] T. Carter, S. A. Seah, B. Long, B. Drinkwater, and S. Subramanian, "UltraHaptics: Multi-point mid-air haptic feedback for touch surfaces," in *Proc. 26th Annu. ACM Symp. User Interface Softw. Technol.*, Andrews, U.K., Oct. 2013, pp. 505–514.
[12] B. Long, S. A. Seah, T. Carter, and S. Subramanian, "Rendering 3D haptic shapes in mid-air using ultrasound," *ACM Trans. Graph.*, vol. 33, no. 6, 2014, Art. no. 181.
[13] G. Shakeri, J. H. Williamson, and S. Brewster, "May the force be with you: Ultrasound haptic feedback for mid-air gesture interaction in cars," in *Proc. 10th Int. Conf. Automot. User Interfaces Interact. Veh. Appl.* Toronto, ON, Canada: Univ. Toronto, Sep. 2018, pp. 1–10.
[14] Y. Liu, X. Li, J. Lai, Z. Zheng, H. Zhu, and M. Li, "Construction of ultrasonic tactile force feedback model in teleoperation robot system," *Sensors*, vol. 21, no. 7, p. 2560, Apr. 2021.
[15] T. Romanus *et al.*, "Mid-air haptic bio-holograms in mixed reality," in *Proc. Int. Normal Labour Birth Res. Conf.*, Ann Arbor, MI, USA, Jun. 2018, pp. 348–352.
[16] J. Chen, F. Yu, Z. Wang, and L. Lin, "Multichannel ultrasound focusing delay control method based on variable-length shift register for airborne ultrasound tactile feedback," *IEEE Access*, vol. 8, pp. 24904–24913, 2020.
[17] S. E. Landsberger, "Design and construction of a cable-controlled, parallel link manipulator," M.S. thesis, Dept. Mech. Eng., Massachusetts Inst. Technol., Cambridge, MA, USA, 1984.
[18] J.-H. Park *et al.*, "A portable intuitive haptic device on a Des. for user-friendly teleoperation of a cable-driven parallel robot," *Appl. Sci.*, vol. 11, no. 9, p. 3823, Apr. 2021.
[19] H. Choi *et al.*, "Intuitive bilateral teleoperation of a cable-driven parallel robot controlled by a cable-driven parallel robot," *Int. J. Control, Autom. Syst.*, vol. 18, no. 7, pp. 1792–1805, Jul. 2020.
[20] D. Surdilovic, J. Zhang, and R. Bernhardt, "STRING-MAN: Wire-robot technology for safe, flexible and human-friendly gait rehabilitation," in *Proc. IEEE 10th Int. Conf. Rehabil. Robot.*, Noordwijk, The Netherlands, Jun. 2007, pp. 446–453.
[21] A. Pott, *Cable-Driven Parallel Robots: Theory and Application*. Cham, Switzerland: Springer-Verlag, 2018.
[22] P. Lambert, L. Da Cruz, and C. Bergeles, "Design, modeling, and implementation of a 7-DOF cable-driven haptic device with a configurable cable platform," *IEEE Robot. Autom. Lett.*, vol. 5, no. 4, pp. 5764–5771, Oct. 2020.
[23] T. Iwamoto, T. Maeda, and H. Shinoda, "Focused ultrasound for tactile feeling display," in *Proc. ICAT*, Tokyo, Japan, Dec. 2001, pp. 1–6.
[24] A. Raza, W. Hassan, T. Ogay, I. Hwang, and S. Jeon, "Perceptually correct haptic rendering in mid-air using ultrasound phased array," *IEEE Trans. Ind. Electron.*, vol. 67, no. 1, pp. 736–745, Jan. 2020.
[25] L. Fan, A. Song, and H. Zhang, "Haptic interface device using cable tension based on ultrasonic phased array," *IEEE Access*, vol. 8, pp. 162880–162891, 2020.
[26] Y. Ochiai, K. Kumagai, T. Hoshi, S. Hasegawa, and Y. Hayasaki, "Cross-field aerial haptics: Rendering haptic feedback in air with light and acoustic fields," in *Proc. CHI Conf. Hum. Factors Comput. Syst.*, San Jose, CA, USA, May 2016, pp. 3238–3247.
[27] A. Pott, T. Bruckmann, and L. Mikelsons, "Closed-form force distribution for parallel wire robots," in *Proc. 5th Int. Workshop Comput. Kinematics*, Duisburg, Germany, May 2009, pp. 25–34.
[28] T. Xue, W. Wang, J. Ma, W. Liu, Z. Pan, and M. Han, "Progress and prospects of multimodal fusion methods in physical human–robot interaction: A review," *IEEE Sensors J.*, vol. 20, no. 18, pp. 10355–10370, Sep. 2020.
[29] R. Takahashi, L. Hasegawa, and H. Shinoda, "Lateral modulation of midair ultrasound focus for intensified vibrotactile stimuli," in *Proc. 11th Int. Conf. EuroHaptics*, Pisa, Italy, Jun. 2018, pp. 276–288.
[30] D. Vaquero-Melchor and A. M. Bernardos, "Enhancing interaction with augmented reality through mid-air haptic feedback: Architecture design and user feedback," *Appl. Sci.*, vol. 9, no. 23, p. 5123, Nov. 2019.
[31] J. J. Zwislocki and D. A. Goodman, "Absolute scaling of sensory magnitudes: A validation," *Perception Psychophys.*, vol. 28, no. 1, pp. 28–38, Jan. 1980.
[32] L. A. Jones and H. Z. Tan, "Application of psychophysical techniques to haptic research," *IEEE Trans. Haptics*, vol. 6, no. 3, pp. 268–284, Jul. 2013.

Liqiang Fan received the B.S. degree in automatic from the Nanjing University of Information Science & Technology, Nanjing, China, in 2012, and the M.S. degree in control theory and control engineering from Hohai University, Nanjing, in 2016. He is currently pursuing the Ph.D. degree with the School of Instrument Science and Engineering, Southeast University, Nanjing. His current research interests are haptic interface and force feedback.

Aiguo Song (Senior Member, IEEE) received the B.S. degree in automatic control in 1990, the M.S. degree in measurement and control from the Nanjing University of Aeronautics and Astronautics, Nanjing, China, in 1993, and the Ph.D. degree in measurement and control from Southeast University, Nanjing, in 1998. He was an Associate Researcher with the Intelligent Information Processing Laboratory, Southeast University, where he was an Associate Professor with the Department of Instrument Science and Engineering, from 1998 to 2000. From 2000 to 2003, he was the Director of the Robot Sensor and Control Laboratory, Southeast University. From April 2003 to April 2004, he was a Visiting Scientist with the Laboratory for Intelligent Mechanical Systems, Northwestern University, Evanston, IL, USA. He is currently a Professor with the School of Instrument Science and Engineering, Southeast University. His major interests concentrate on teleoperation control, haptic display, internet telerobotics, and distributed measurement systems.

Haochen Zhang received the B.S. degree in automatic from Northeastern University, Shenyang, China, in 2009, and the M.S. degree in control theory and control engineering from the Lanzhou University of Technology, Lanzhou, China, in 2013. He is currently pursuing the Ph.D. degree with the School of Instrument Science and Engineering, Southeast University, Nanjing, China. His current research interests are teleoperation control and robot control.